Eur. Phys. J. C (2014) 74:2745
DOI 10.1140/epjc/s10052-014-2745-2

THE EUROPEAN PHYSICAL JOURNAL C

Regular Article - Theoretical Physics

Drell–Yan, ZZ, W^+W^- production in SM & ADD model to NLO+PS accuracy at the LHC

R. Frederix[1,a], **M. K. Mandal**[2,b], **P. Mathews**[3,c], **V. Ravindran**[4,d], **S. Seth**[3,e]

[1] TH Unit, PH Department, CERN, 1211 Geneva 23, Switzerland
[2] Regional Centre for Accelerator-based Particle Physics, Harish-Chandra Research Institute, Chhatnag Road, Jhunsi, Allahabad 211 019, India
[3] Saha Institute of Nuclear Physics, 1/AF Bidhan Nagar, Kolkata 700 064, India
[4] The Institute of Mathematical Sciences, C.I.T Campus, 4th Cross St, Tharamani, Chennai, Tamil Nadu 600 113, India

Received: 30 July 2013 / Accepted: 16 January 2014 / Published online: 7 February 2014

Abstract In this paper, we present the next-to-leading order QCD corrections for di-lepton, di-electroweak boson (ZZ, W^+W^-) production in both the SM and the ADD model, matched to the HERWIG parton shower using the aMC@NLO framework. A selection of results at the 8 TeV LHC, which exhibit deviations from the SM as a result of the large extra-dimension scenario, are presented.

1 Introduction

With more accumulated data at the LHC, extra-dimension searches at different energies have yielded stringent bounds [1,2] on the model parameters [3–6]. This has also been facilitated by improved theoretical calculations to next-to-leading order (NLO) in QCD that have been available for the large (ADD) [3–5] and warped (RS) [6] extra-dimension models for various processes *viz.* di-lepton [7–9], di-boson ($\gamma\gamma$ [10,11], ZZ [12–14], WW [15,16] (W^+W^- is denoted as WW)). In extra-dimension models, pair production could result from the exchange of virtual Kaluza–Klein (KK) modes. As a result of possible new physics, it is expected that the production rate and potentially certain kinematical distributions may get modified as compared to the SM predictions. Further, it is essential that higher order QCD corrections are included as they lead to reduction in scale uncertainties, which in turn improves the theoretical predictions. For extra-dimension searches, ATLAS and CMS have investigated the impact of NLO corrections in their analysis by using constant K-factors, which does not necessarily give reliable predictions.

One important recent development has been the implementation of the di-photon production to NLO including Parton Shower (PS) in the aMC@NLO environment for the ADD model [17]. This allows for the generation of fully exclusive events that are NLO accurate for observables inclusive in QCD radiation. If required, these events can be directly passed through a detector simulation. In this paper, we have implemented the rest of the pair production processes ($\ell^+\ell^-$, ZZ and WW) that could contribute to the ADD model, to NLO+PS accuracy in the aMC@NLO environment.

To set the notations and the conventions used, we briefly describe the interaction Lagrangian,

$$\mathcal{L}_{\rm int} = -\frac{\kappa}{2}\sum_{(\vec{n})} T^{\mu\nu} h^{(\vec{n})}_{\mu\nu}, \tag{1}$$

of the massive spin-2 KK modes $h^{(\vec{n})}_{\mu\nu}$ with the SM particles, which is through the energy momentum tensor $T^{\mu\nu}$ of the SM. The coupling κ is related to the Planck mass in 4-dimension, $\kappa = \sqrt{16\pi}/M_P$. Using the convention of HLZ [18] the summation of the KK modes in the propagator $\mathcal{D}(s)$ is given by

$$\begin{aligned}\kappa^2\mathcal{D}(s) &= \kappa^2\sum_n \frac{1}{s - m_n^2 + i\epsilon},\\ &= \frac{8\pi}{M_S^4}\left(\frac{\sqrt{s}}{M_S}\right)^{(d-2)}\left[-i\pi + 2I\left(\frac{\Lambda}{\sqrt{s}}\right)\right].\end{aligned} \tag{2}$$

The summation over KK modes leads to the integral $I(\Lambda/\sqrt{s})$, defined in [18], $\sqrt{s}$ is the center of mass energy, and Λ is the UV cutoff of the KK modes, which is identified with the fundamental scale M_S in $4+d$ dimensions [18,19]. Bounds on M_S for different extra dimensions d have been

[a] e-mail: rikkert.frederix@cern.ch
[b] e-mail: mandal@hri.res.in
[c] e-mail: prakash.mathews@saha.ac.in
[d] e-mail: ravindra@imsc.res.in
[e] e-mail: satyajit.seth@saha.ac.in

obtained by the ATLAS and CMS collaborations; for our present analysis we choose the following values: $M_S = 3.7$ TeV ($d = 2$), 3.8 TeV ($d = 3$), 3.2 TeV ($d = 4$), 2.9 TeV ($d = 5$), 2.7 TeV ($d = 6$).

The rest of the paper is as follows: we briefly describe the framework for matching the NLO results with Parton Shower Monte Carlo in Sect. 2. A selection of the numerical results are presented in Sect. 3, and finally we present our conclusions in Sect. 4.

2 NLO+PS

In order to provide a more realistic description of a process at the LHC, it is unavoidable to match the NLO QCD results with Parton Shower Monte Carlo. For the present analysis, we adopt the MC@NLO formalism [20] to match the fixed order NLO results with the HERWIG6 [21] parton shower, including the hadronization contribution by using the automated aMC@NLO framework. The Born and real-emission correction for all these processes are computed with MadFKS [22], which uses the FKS subtraction method [23] to compute the real-emission contribution in an automated way, within the MadGraph5 [24] environment. The virtual contributions are implemented separately in this environment for each of these processes, using the analytically calculated results for $\ell^+\ell^-$ [7–9], ZZ [12–14], and WW [15,16] production processes. We have also incorporated an algorithm that takes care of the summation of the KK modes in the ADD model (Eq. 2); this has been made possible by appropriate changes in the spin-2 HELAS routine [17]. The exact numerical cancelations of double and single poles coming from the real and virtual terms in all the subprocesses, for each of the production processes have been checked.

For the Drell-Yan (DY) process, we have generated the events for the process $PP \to e^+e^- X$, which is phenomenologically same as $PP \to \mu^+\mu^- X$, except for the experimental identification of the final state particles. The leading order (LO) partonic contribution comes from the $q\ \bar{q} \to e^+e^-$ in both the SM and the ADD model, whereas at LO $g\ g \to e^+e^-$ contributes only to the ADD model. Emission of real gluon and one loop correction due to the virtual gluon, together with the partonic subprocess $q(\bar{q})\ g \to q(\bar{q})\ e^+e^-$, give all the $\mathcal{O}(\alpha_s)$ contributions. The interference between the SM and ADD diagrams also give $\mathcal{O}(\alpha_s)$ contribution at the NLO. For the di-boson final states, in addition to similar partonic sub processes, there are contributions due to the interference between the gg initiated box diagrams in SM and the gg initiated Born diagrams in the ADD which is of $\mathcal{O}(\alpha_s)$. We have considered all the above contributions in each of these processes of interest for our present analysis.

After generation of events following the above procedure, we let the Z and $W^\pm$ bosons to decay to leptons at the time of showering. For the ZZ events, we let one Z boson decay to e^+e^- and the other one to $\mu^+\mu^-$, while for the WW events we let the W^+ decay to $e^+\nu_e$ and the W^- to $\mu^-\bar{\nu}_\mu$. Alternatively, the $W^\pm$ and Z bosons can be decayed using MadSpin [25] at the time of event generation itself, which retains nearly all spin correlations. We have not chosen to do this, because the inclusion of the sum over the KK modes is non-trivial in this way.

3 Numerical result

In this section, we present some of the kinematical distributions for the production of $\ell^+\ell^-$, ZZ, WW, both in the SM and ADD to NLO+PS accuracy for the LHC center of mass energy $\sqrt{S} = 8$ TeV. Events are generated using the following input parameters: $\alpha_{EW}^{-1} = 132.507$, $G_F = 1.16639 \times 10^{-5}\,\text{GeV}^{-2}$, $m_z = 91.188\,\text{GeV}$. Using these electroweak parameters as inputs, the mass of W boson $m_w = 80.419\,\text{GeV}$ and $\sin^2\theta_w = 0.222$ are obtained. The (N)LO events are generated using MSTW(n)lo2008cl68 parton distribution functions (PDF) for the (N)LO and the value of strong coupling constant α_s is solely determined by the corresponding MSTW PDF [26] at (N)LO. The factorization scale μ_F and the renormalization scale μ_R are set equal to the invariant mass of the corresponding di-final state. The number of active quark flavors is taken to be five and they are treated as massless. We use the following loose cuts at the time of event generation for the DY production: (a) transverse momentum of the lepton $P_T^\ell > 15$ GeV, (b) rapidity $|\eta^\ell| < 2.7$, (c) the separation of two particles in the rapidity–azimuthal angle plane $\Delta R^{e^+e^-} > 0.3$ (where $\Delta R = \sqrt{(\Delta\eta)^2 + (\Delta\phi)^2}$) and (d) the invariant mass $M_{e^+e^-} < 1.1 \times M_S$. For ZZ and WW event generation, we use no cut at the generation level except on the invariant mass *i.e.*, $M_{ZZ}, M_{W^+W^-} < 1.1 \times M_S$. For WW event generation, the following CKM matrix elements are used: $|V_{ud}| = 0.97425$, $|V_{us}| = 0.2252$, $|V_{ub}| = 4.15 \times 10^{-3}$, $|V_{cd}| = 0.230$, $|V_{cs}| = 1.006$, $|V_{cb}| = 40.9 \times 10^{-3}$. All the CKM matrix elements associated with the top quark are taken to be zero.

For showering the DY events, HERWIG6 in MC@NLO formalism is used. Using the following analysis cuts: $P_T^l > 20\,\text{GeV}$ ($l = e^+, e^-$), $|\eta^l| < 2.5$, $M_{e^+e^-} < M_S$, $\Delta R^{ll} > 0.4$ for showering, the hardest (with maximum P_T) e^+ and e^- are collected. In order to separate leptons from jets, $\Delta R^{lj} > 0.7$ is used. For both ZZ and WW showering, we have identified those final state, stable lepton pairs, whose mother is one of the Z boson (for ZZ showering) or the final state stable lepton–neutrino pair whose mother is one of the W boson (for WW showering). That is the reason why we avoid the cut which is commonly used to reconstruct the $Z(W)$ boson mass from the invariant mass of the lepton-lepton (lepton-neutrino) pair. For decay products of Z/W, we use the same analysis cuts to plot various differential distributions, namely the fol-

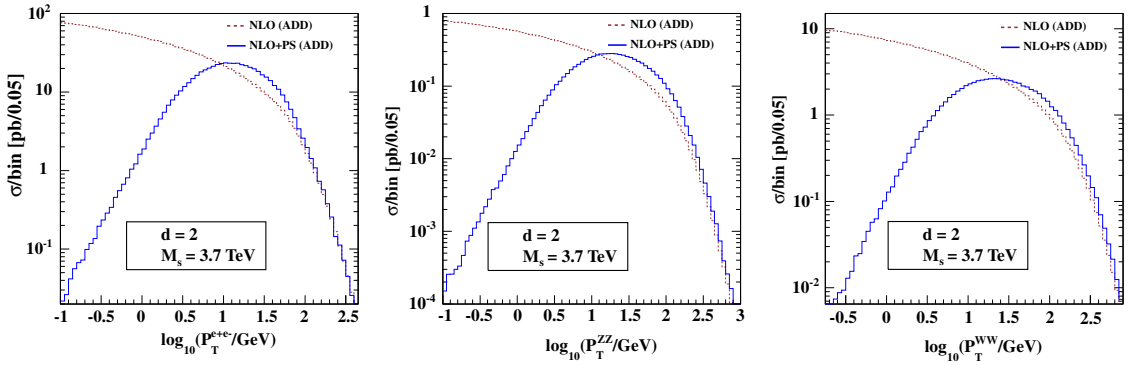

Fig. 1 Fixed order NLO results (*dashed brown*) along with the NLO+PS results (*solid blue*) for the $\log_{10}(P_T)$ distribution of the e^+e^- (*left*), ZZ (*middle*), and W^+W^- (*right*) pair

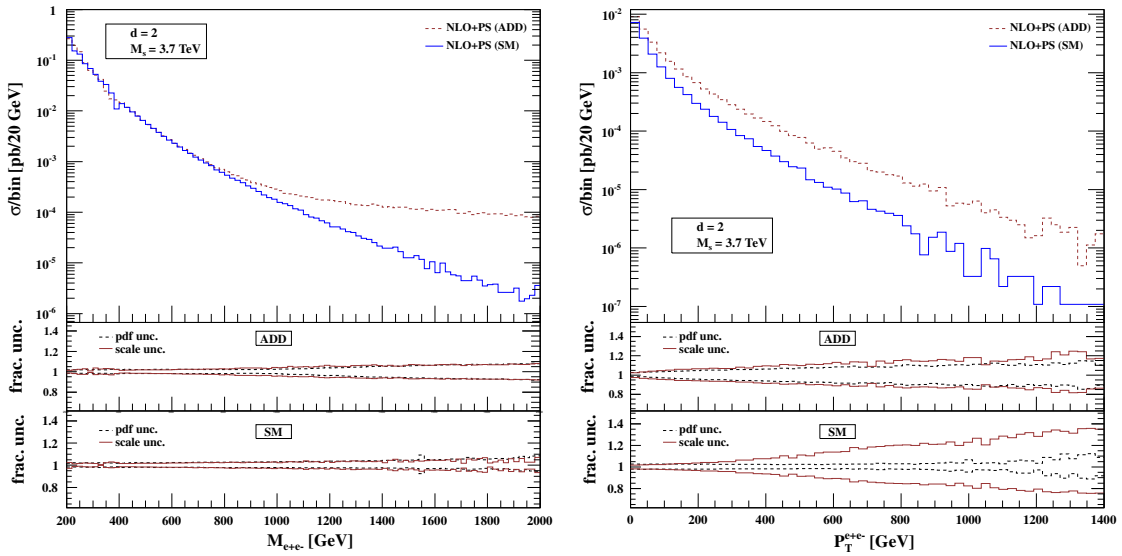

Fig. 2 Invariant mass ($M_{e^+e^-}$) distribution (*left*) and transverse momentum distribution (*right*) of the e^+e^- pair for ADD ($d = 2$) and SM in Drell–Yan process. The *right one* is in the $M_{e^+e^-} > 600\,\text{GeV}$ region

lowing: invariant mass $M_{ZZ/W^+W^-} < M_S$, $P_T^l > 20\,\text{GeV}$ (where $l = e^+, e^-, \mu^+, \mu^-$ for ZZ and $l = e^+, \mu^-$ for W^+W^-), $|\eta^l| < 2.5$. In addition, we have collected only those leptons whose separations from other leptons and jets are greater than 0.4 and 0.7, respectively, in the rapidity–azimuthal angle plane.

Here, we describe few selected differential distributions for some of the kinematical observables. To start with, we study the effect of parton shower over the fixed order NLO correction. Fixed order NLO results (dashed brown) along with the NLO+PS results (solid blue) for the $\log_{10}(P_T)$ distribution of the e^+e^- (left), ZZ (middle), and WW (right) pair are plotted in Fig. 1, using their specific analysis cuts detailed above for extra dimensions $d = 2$ and its corresponding M_S value. In all these plots, the fixed order cross section diverges for $P_T \to 0$, while the NLO+PS result shows a converging behavior in the low P_T region. The effect of parton shower ensures correct resummation of the Sudakov logarithmic terms which appear in the collinear region leading to a suppression of the cross section in the low P_T region. There is no significant deviation in the high P_T region as expected.

In the subsequent plots, we have included fractional scale and PDF uncertainties corresponding to the SM and ADD model distributions. By fractional uncertainty we mean the central value of a particular distribution divided by its extremum value. The scale uncertainties are calculated by considering independent variation of the renormalization and the factorization scales in the following way: $\mu_R = \xi_R M$ and $\mu_F = \xi_F M$. Here, M denotes the invariant mass of the di-final state *i.e.*, $M_{e^+e^-}, M_{ZZ}, M_{WW}$ as required and ξ_R, ξ_F can take either of the values $(1, 1/2, 2)$ independently. The scale uncertainty band is the envelope of the following (ξ_F, ξ_R) combinations [17] as described below: (1, 1), (1/2, 1/2), (1/2, 1), (1, 1/2), (1, 2), (2, 1), (2, 2). The estimation of the PDF uncertainty is done in the Hessian method as prescribed by the MSTW [26] collaboration. All these uncer-

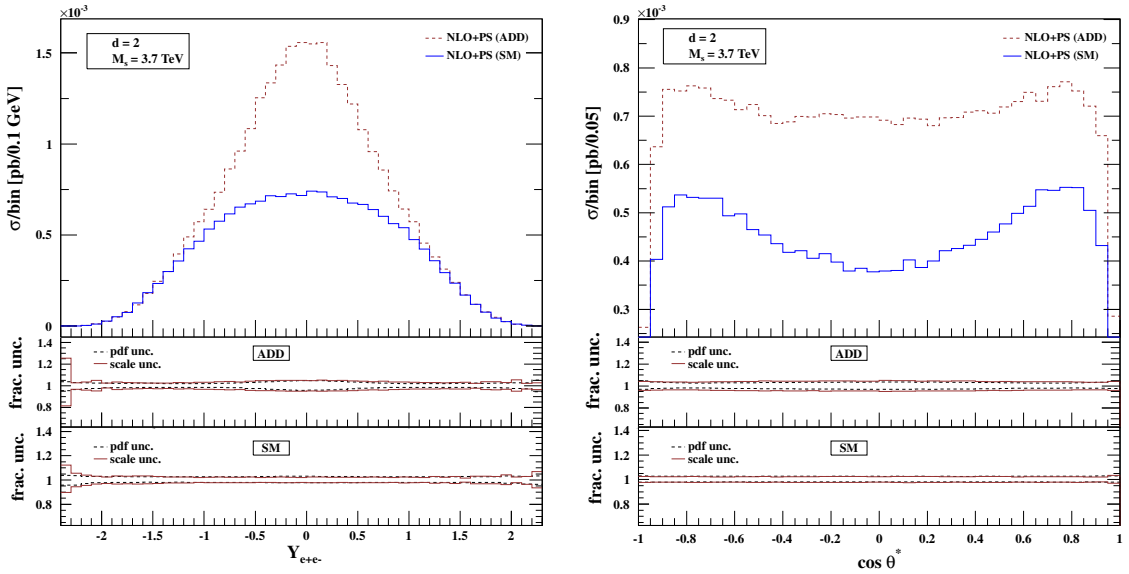

Fig. 3 Rapidity distribution (*left*) of e^+e^- pair and the angular distribution (*right*) are given for $d = 2$ in ADD and also for SM in Drell–Yan process for $M_{e^+e^-} > 600\,\text{GeV}$

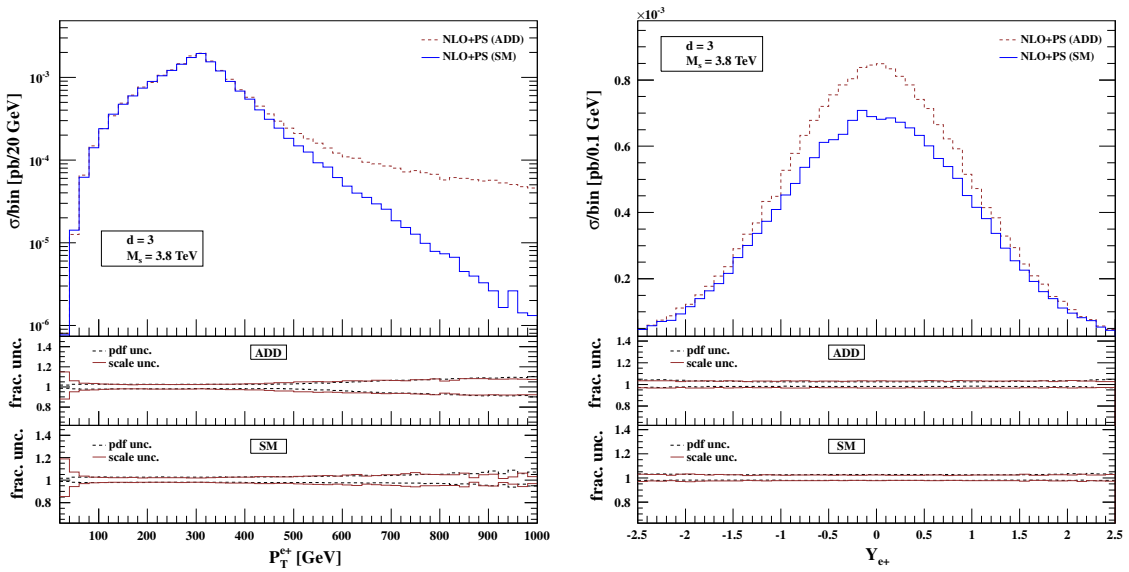

Fig. 4 Transverse momentum (*left*) and rapidity (*right*) distribution of final state positron in ADD ($d = 3$) and SM for Drell–Yan process for $M_{e^+e^-} > 600\,\text{GeV}$

tainties are determined automatically by following the reweighting procedure [27] built in aMC@NLO which stores sufficient information in the parton level Les Houches events for this purpose.

In all the plots ADD represents the full contribution of the SM and ADD model contributions including interference. We use a consistent graphical representation for the rest of the kinematic distributions. In each case, the upper inset gives the distribution in the SM (solid blue) as well as in the ADD model (dashed brown) to NLO+PS accuracy. For the same distribution, the middle (ADD) and lower (SM) insets provide fractional scale (solid brown) and PDF (dashed black) uncertainties.

Various kinematical observable in the DY process are given in Figs. 2, 3, 4 and 5. In Fig. 2, we have shown the invariant mass distribution (left) and transverse momentum distribution (right) of the e^+e^- pair for $d = 2$ with its associated M_S value. The effect of a large extra dimension is dominant in the high invariant mass region and hence we focus on the region $M_{e^+e^-} > 600\,\text{GeV}$ to study the other distribution *viz.* P_T, rapidity, angular distribution of the e^+e^- pair and also look at some of the distributions of the individual lep-

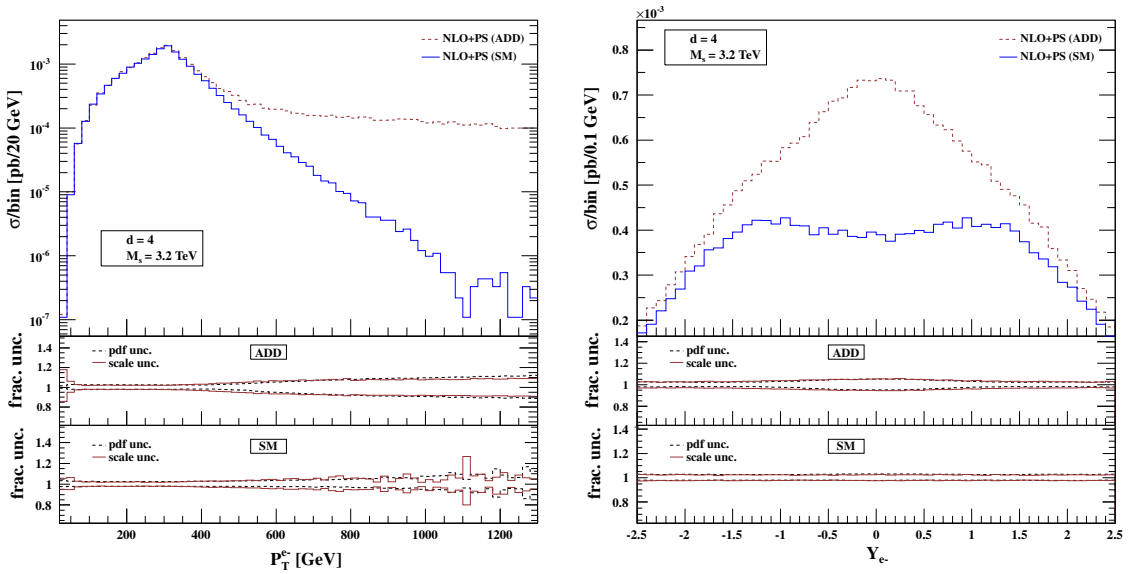

Fig. 5 Transverse momentum (*left*) and rapidity (*right*) distribution of final state electron in ADD ($d = 4$) and SM for Drell–Yan process for $M_{e^+e^-} > 600\,\text{GeV}$

tons. In Fig. 2, note that there is an increase in the scale and PDF uncertainties with increase in P_T as is well known, see for example [28]. In Fig. 3, the rapidity distribution of e^+e^- pair (left) and the angular distribution (right) are given for $d = 2$. For the rapidity distribution the deviation from the SM is only prominent in the central region. The angle made by the lepton pair in its center of mass frame with respect to one of the incoming hadron is denoted by θ^*. The angular distribution is a good discriminator for the full range to distinguish the ADD from the SM. Figure 4 describes the behavior of P_T (left) and rapidity (right) distribution of final state positron for $d = 3$ extra dimensions. Similarly, in Fig. 5, transverse momentum distribution (left) is presented along with the rapidity distribution (right) of the final state electron for $d = 4$. The difference in the SM rapidity distribution for e^- (Fig. 4) compared to e^+ (Fig. 5), can be attributed to the fact that Z boson couples differently to left and right handed fermions and the high invariant mass cut used to zoom into the region of interest for the ADD model, enhances this effect.

The plots associated with the decay products of ZZ process are presented in Figs. 6, 7, 8. For $d = 2$ we see deviations from the SM in the high invariant mass region in the case of four-lepton invariant mass (M_{4l}) distribution as shown in Fig. 6. Except for the invariant mass distribution, all other kinematical observable are studied above the region where the four-lepton invariant mass is greater than 600 GeV, which is the ADD dominant region. In Fig. 7, we show transverse momentum (left) and rapidity (right) distribution of the e^+e^- pair for $d = 3$. Similarly, the transverse momentum (left) and rapidity (right) distribution for the $\mu^+\mu^-$ pair are presented in Fig. 8 for $d = 4$. The ADD distributions are fairly distinguishable for $d = 4$ compared to $d = 3$, as bounds on M_S value for larger number of extra dimensions is a bit lower.

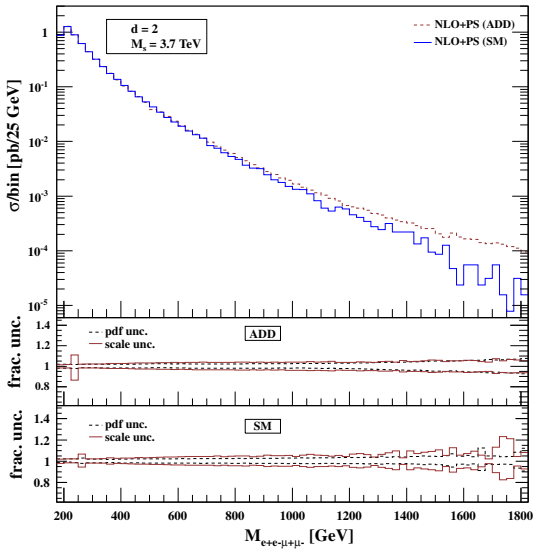

Fig. 6 Four-lepton invariant mass (M_{4l}) distribution for ADD ($d = 2$) and SM for decay products coming from the ZZ process

For the WW production process, the relevant plots are presented in Figs. 9 and 10, wherein the decays of $W^\pm$ bosons to leptons and neutrinos are included at the stage of showering. For the choice of M_S values associated with specific number of extra dimensions, we do not find any significant deviation from the SM. In the very high invariant mass region of the four-body final state for $d = 5, 6$ there is some deviation form the SM. In Fig. 9, we have given

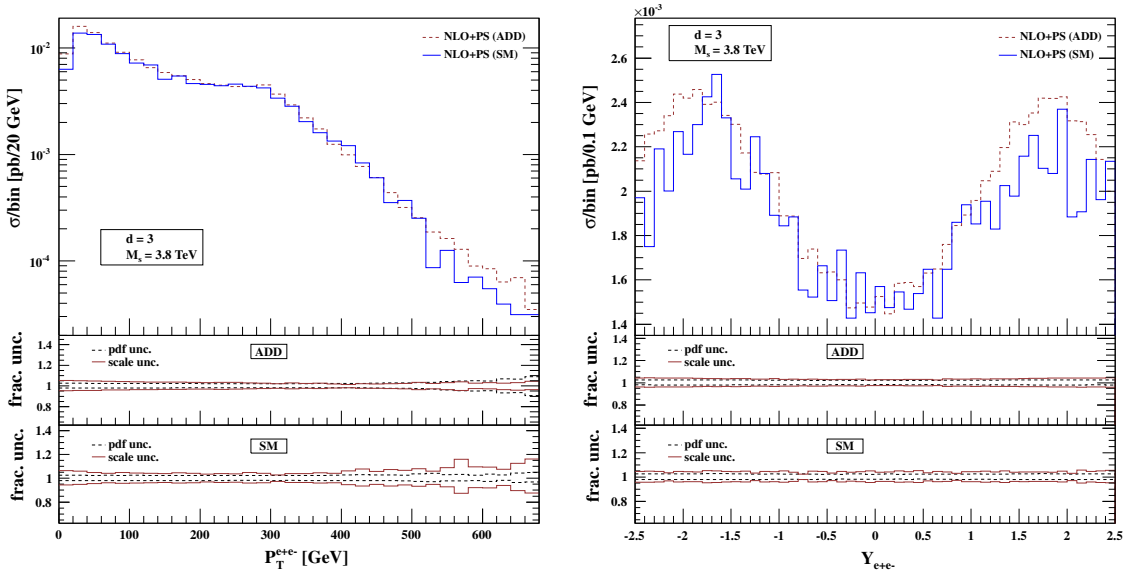

Fig. 7 Transverse momentum (*left*) and rapidity (*right*) distribution of the e^+e^- pair coming from ZZ decay for ADD ($d = 3$) and SM, when $M_{4l} > 600\,\text{GeV}$

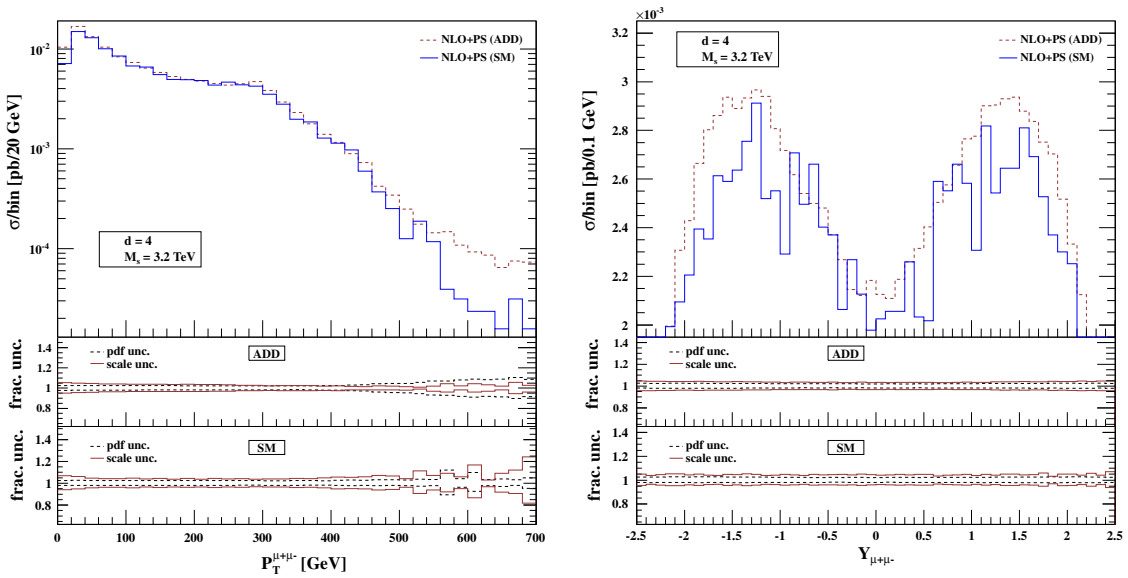

Fig. 8 Transverse momentum (*left*) and rapidity (*right*) distribution of the $\mu^+\mu^-$ pair coming from ZZ decay for ADD ($d = 4$) and SM, when $M_{4l} > 600\,\text{GeV}$

the invariant mass ($M_{e^+\mu^-\not{E}_T}$) distribution (left) of the final state decay products of $\tilde{W}^{\pm}$ and the total missing transverse energy distribution (right) which comes from the final state neutrinos for $d = 5$. For completeness in Fig. 10, we also provide the transverse momentum distribution of the final state positron (left) along with its rapidity distribution (right) for $d = 6$. Only a mild difference between the SM and ADD in the high invariant mass region is observed. We zoom in into this very high invariant mass region to look for deviations from the SM for these exclusive observable. We have studied $d\sigma/d\not{E}_T$, $d\sigma/dP_T^{e^+}$, and $d\sigma/d\eta_{e^+}$ in the region where the invariant mass lies between 2 TeV and M_S.

Using the di-lepton process, we present the search sensitivity for the extra dimensions $d = 2$–6, for 14 TeV LHC. The total cross section σ is calculated using the invariant mass distribution of the di-lepton pair for signal plus background and the background only. For a particular choice of the extra dimension d, we find the minimum luminosity by varying the scale M_S at 3-sigma and 5-sigma signal significance. We define the required minimum luminosity as $L = \max\{L_{3\sigma(5\sigma)}, L_{3N_S(5N_S)}\}$, where $L_{3\sigma(5\sigma)}$ is the inte-

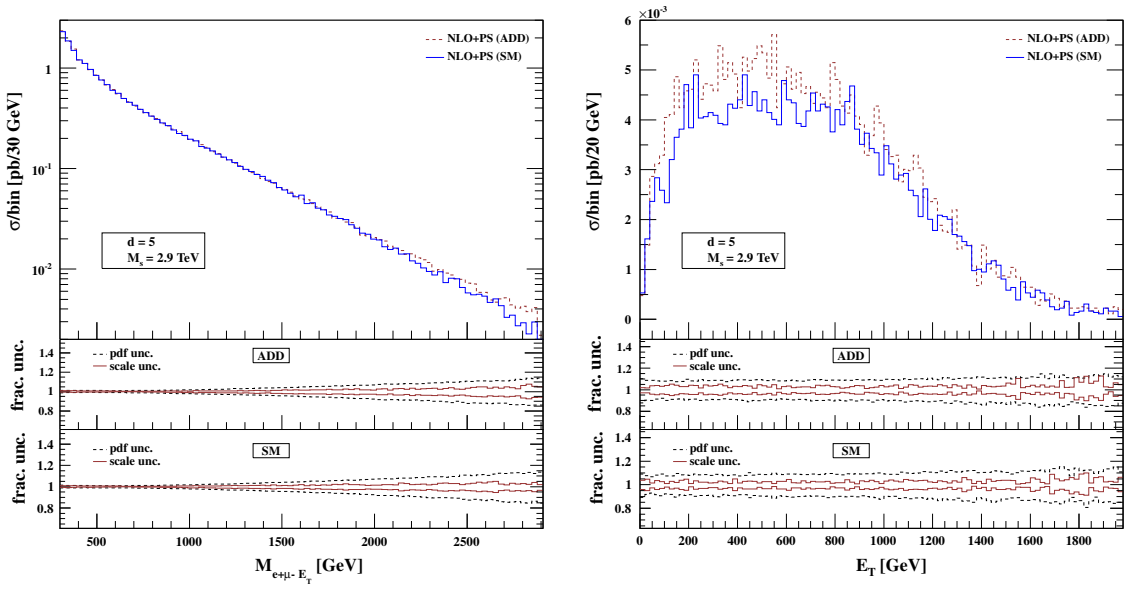

Fig. 9 Invariant mass ($M_{e^+\mu^-\not{E}_T}$) distribution (*left*) of all the final state decay products of WW and the total missing transverse energy distribution (*right*) for ADD ($d = 5$) and SM. The right one is restricted within $2000 < M_{e^+\mu^-\not{E}_T} < M_S$ GeV

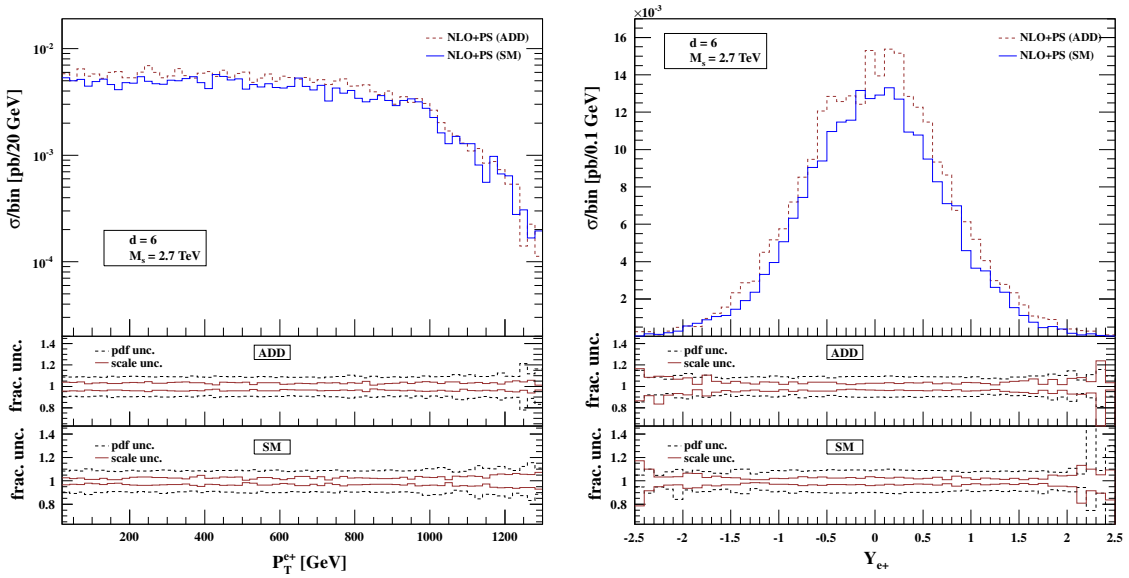

Fig. 10 Transverse momentum distribution (*left*) and rapidity distribution (*right*) of the final state positron which comes from W^+ decay for WW production process in both ADD ($d = 6$) and SM when $2000 < M_{e^+\mu^-\not{E}_T} < M_S$ GeV

grated luminosity at 3-sigma (5-sigma) signal significance and $L_{3N_S(5N_S)}$ describes the integrated luminosity to get at least 3(5) signal events. Now we can get the corresponding M_S value for 10 fb^{-1} luminosity by inversion which is tabulated in Table 1. Of course, a full analysis including the effects of detector simulation, non-reducible backgrounds *etc.* can be better performed by the experimental collaborations.

Table 1 Lower bounds on M_S for various extra dimensions d at the 14 TeV LHC with integrated luminosity of 10 fb^{-1} at 3-sigma and 5-sigma signal significance

d	2	3	4	5	6
$M_S^{(3\sigma)}$ (TeV)	12.3	13.7	13.5	11.3	10.5
$M_S^{(5\sigma)}$ (TeV)	10.8	11.3	11.1	11.2	10.1

4 Conclusion

The main objective of this work has been to make available, the $\ell^+\ell^-$, ZZ, W^+W^- production results to NLO+PS accuracy for the large extra-dimension model which is implemented in the aMC@NLO framework. All the subprocesses that contribute to NLO in QCD have been included for each of these processes. A selection of results for 8 TeV LHC has been presented for various distributions in an attempt to identify the region of interest for extra-dimension searches. Scale and PDF uncertainties for each of these distributions have also been studied. In addition, we have presented the search sensitivity for the extra dimensions $d = 2$–6, for 14 TeV LHC at 10 fb^{-1}. With the earlier implementation of the di-photon final state to the same accuracy [17], this work completes the rest of the di-final state process (but for di-jet) in large extra-dimension searches. In the ADD model, these codes can be used to generate events of the di-final states discussed in this paper to NLO+PS accuracy and are available on the website http://amcatnlo.cern.ch.

Acknowledgements The work of MKM and VR has been partially supported by funding from Regional Center for Accelerator-based Particle Physics (RECAPP), Department of Atomic Energy, Govt. of India. We would like to thank the High Performance Computing cluster at Theory Division, SINP, where the computational work was carried out.

References

1. C.M.S. Collaboration, Phys. Rev. Lett. **108**, 111801 (2012)
2. ATLAS Collaboration, Phys. Lett. B **710**, 538 (2012)
3. N. Arkani-Hamed, S. Dimopoulos, G. Dvali, Phys. Lett. B **429**, 263 (1998)
4. I. Antoniadis, N. Arkani-Hamed, S. Dimopoulos, G. Dvali, Phys. Lett. B **436**, 257 (1998)
5. N. Arkani-Hamed, S. Dimopoulos, G. Dvali, Phys. Rev. D **59**, 086004 (1999)
6. L. Randall, R. Sundrum, Phys. Rev. Lett. **83**, 3370 (1999)
7. P. Mathews, V. Ravindran, K. Sridhar, W.L. van Neerven, Nucl. Phys. B **713**, 333 (2005)
8. P. Mathews, V. Ravindran, Nucl. Phys. B **753**, 1 (2006)
9. M.C. Kumar, P. Mathews, V. Ravindran, Eur. Phys. J. C **49**, 599 (2007)
10. M.C. Kumar, P. Mathews, V. Ravindran, A. Tripathi, Phys. Lett. B **672**, 45 (2009)
11. M.C. Kumar, P. Mathews, V. Ravindran, A. Tripathi, Nucl. Phys. B **818**, 28 (2009)
12. N. Agarwal, V. Ravindran, V.K. Tiwari, A. Tripathi, Nucl. Phys. B **830**, 248 (2010)
13. N. Agarwal, V. Ravindran, V.K. Tiwari, A. Tripathi, Phys. Lett. B **686**, 244 (2010)
14. N. Agarwal, V. Ravindran, V.K. Tiwari, A. Tripathi, Phys. Rev. D **82**, 036001 (2010)
15. N. Agarwal, V. Ravindran, V.K. Tiwari, A. Tripathi, Phys. Rev. D **82**, 036001 (2010)
16. N. Agarwal, V. Ravindran, V.K. Tiwari, A. Tripathi, Phys. Lett. B **690**, 390 (2010)
17. R. Frederix, M.K. Mandal, P. Mathews, V. Ravindran, S. Seth, P. Torrielli, M. Zaro, JHEP **1212**, 102 (2012)
18. T. Han, J.D. Lykken, R.J. Zhang, Phys. Rev. D **59**, 105006 (1999)
19. G.F. Giudice, R. Rattazzi, J.D. Wells, Nucl. Phys. B **544**, 3 (1999)
20. S. Frixione, B.R. Webber, JHEP **0206**, 029 (2002)
21. G. Corcella, I.G. Knowles, G. Marchesini, S. Moretti, K. Odagiri, P. Richardson, M.H. Seymour, B.R. Webber, JHEP **01**, 010 (2001)
22. R. Frederix, S. Frixione, F. Maltoni, T. Stelzer, JHEP **10**, 003 (2009)
23. S. Frixione, Z. Kunszt, A. Signer, Nucl. Phys. B **467**, 399–442 (1996)
24. J. Alwall, M. Herquet, F. Maltoni, O. Mattelaer, T. Stelzer, JHEP **1106**, 128 (2011)
25. P. Artoisenet, R. Frederix, O. Mattelaer, R. Rietkerk, JHEP **1303**, 015 (2013)
26. A.D. Martin, W.J. Stirling, R.S. Thorne, G. Watt, Eur. Phys. J. C **63**, 189–285 (2009)
27. R. Frederix, S. Frixione, V. Hirschi, F. Maltoni, R. Pittau et al., JHEP **1202**, 099 (2012)
28. P. Torrielli, S. Frixione, JHEP **1004**, 110 (2010)